A continuum-oriented finite-discrete element method (cFDEM) for rock fracturing simulation

Ke Gao
Department of Earth and Space Sciences, Southern University of Science and Technology, Shenzhen, Guangdong, China

Weibing Cai
Department of Earth and Space Sciences, Southern University of Science and Technology, Shenzhen, Guangdong, China

Shugang Ai
Department of Earth and Space Sciences, Southern University of Science and Technology, Shenzhen, Guangdong, China

ABSTRACT: The combined finite-discrete element method (FDEM) has been extensively used for rock fracturing simulation. The zero-thickness intrinsic cohesive elements are commonly implemented in FDEM and pre-inserted in the rock model between adjacent finite elements prior to simulation. However, because of the different constitutive laws for cohesive and finite elements, the rock model domain may deform like a discontinuum in the elastic stage (abbreviated as dFDEM). This could cause unrealistic material deformation and also reduce computational efficiency. Here, we propose a novel node binding algorithm to ensure the continuum behavior of materials prior to fracture onset (abbreviated as cFDEM), which can also automatically achieve the explicit separation of fracture surfaces without using complex node splitting algorithm. We validate the robustness of the proposed cFDEM and demonstrate its advantage compared to dFDEM. The work provides a novel perspective for rock fracturing simulation in FDEM.

Keywords: Combined finite-discrete element method (FDEM), Node binding algorithm, Rock fracture, Numerical simulation, Cohesive zone model.

1 INTRODUCTION

The combined finite-discrete element method (FDEM) (Munjiza, 1992), which merges FEM-based analysis of continua with DEM-based contact processing for discontinua, provides an effective solution to simulate the fracturing behavior in rocks. Generally, the FDEM is realized using the intrinsic cohesive zone model (ICZM) with a traction-separation law, in which the modeling domain is first discretized into a series of finite elements, and then cohesive elements are inserted into the common boundaries between adjacent finite elements (Munjiza, 2004).

Because finite elements and intrinsic cohesive elements use different types of constitutive laws, they deform at different rates even in the elastic deformation stage, and thus may cause discontinuous strains across adjacent finite elements and make the originally continuous model domain behave like a discontinuum before fracture onset (for convenience, it is referred to as dFDEM hereafter. Since the inherent stiffness difference between the intrinsic cohesive elements and the solid finite elements,

the dFDEM usually yields a smaller overall material elastic modulus than the true value, i.e., stiffness reduction, or the so-called artificial compliance problem (Xu et al., 2022).

To overcome the aforementioned deficiencies in traditional dFDEM, Fukuda et al. (2020) recently introduced the extrinsic cohesive zone model (ECZM) in FDEM, where cohesive elements are adaptively inserted between adjacent finite elements. Compared with dFDEM, this type of FDEM realization is more continuum-oriented, and is thus abbreviated as cFDEM for later reference. However, the adaptive insertion of cohesive elements requires a robust algorithm for splitting the local nodes between adjacent finite elements.

To circumvent the disadvantages of the ICZM-based dFDEM and the ECZM-based cFDEM, we propose a novel 2D realization of cFDEM using the cohesive zone model implemented in our in-house FDEM code – Pamuco. Specifically, similar to dFDEM, we first discretize the numerical model domain into finite elements and re-joint them with cohesive elements; then, we use a node binding scheme, in a master-slave manner, to bind nodes that share the same original coordinates. The proposed cFDEM realization suppresses the calculation of cohesive elements prior to fracture onset, which ensures the continuum behavior of the model domain in the elastic stage. When a certain strength criterion is reached, the pre-inserted cohesive element will be invoked. Meanwhile, the node binding lists will be automatically updated to accommodate the explicit separation of fracture surfaces. Essentially, the proposed cFDEM inherits the merits of both ICZM and ECZM, but avoids their shortcomings.

2 FORMULATIONS OF THE PROPOSED CFDEM

In this section, we first propose a novel node binding scheme that ensures the equivalent continuum behavior of the model domain in the elastic deformation stage. Following this, we demonstrate the realization of fracture initiation and propagation in cFDEM.

2.1 Elastic deformation and node binding scheme

To avoid frequent updating of element topology information when new fractures are initiated in the proposed cFDEM, we first borrow the strategies used in the ICZM-based dFDEM for element topology processing. Taking the model presented in Figure 1 for example, we discretize the whole continuous model domain into six triangular finite elements, and then separate them into independent ones (without node sharing) (see Figure 1b).

To prepare for the node binding scheme in a later stage, we also reserve the mapping information from the original nodes before model discretization (denoted as master nodes, e.g., Node *i* in Figure 1a) to the corresponding new nodes after model discretization (denoted as slave nodes, e.g., Nodes 0 to 5 in Figure 1b) in a master-slave manner. Each master node corresponds to several slave nodes, and together they form a master-slave group. This mapping information between the master and slave nodes can be saved in a list such as $0 \rightarrow i$, $1 \rightarrow i$, …, $5 \rightarrow i$ (Figure 1c). If a master node is located inside the model (i.e., not connected to any model boundaries, e.g., Node *i*), all its slave nodes will be stored in a circular linked list according to their relative positions, e.g., $0 \rightarrow 1 \rightarrow 2 \rightarrow 3 \rightarrow 4 \rightarrow 5 \rightarrow 0$ (Figure 1c). However, if a master node is located on the model boundary (e.g., Node *j*), its slave nodes (e.g., Nodes 6, 7) can be stored in an open linked list, e.g., $6 \rightarrow 7$. After model discretization, the original mesh topology information will be abandoned and all later computations are conducted only based on the new element topology.

To avoid the discontinuous elastic deformation similar to that in the ICZM-based dFDEM, we suppress the functionality of pre-inserted cohesive elements during the elastic stage by binding the slave nodes in each group. In other words, the slave nodes in the same group will displace together with their master node, which guarantees pure continuous deformation in areas without yield surfaces.

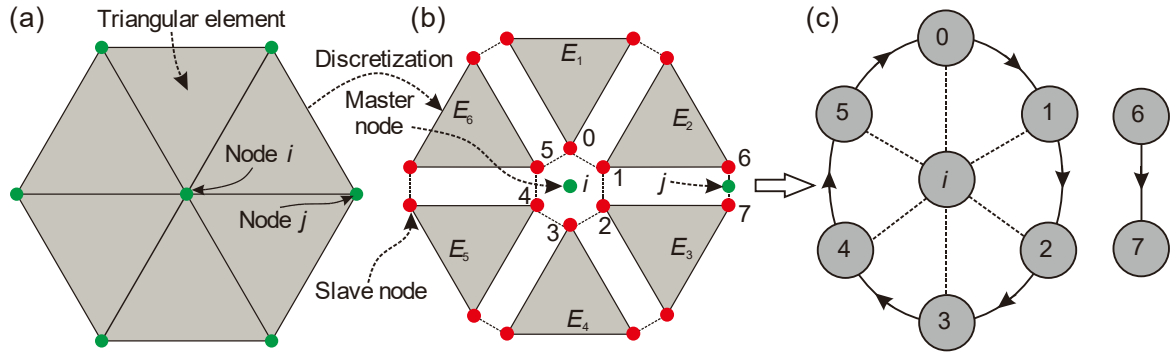

Figure 1. Mesh discretization and re-join of triangular finite elements by cohesive elements. Nodes 0 to 5 are slave nodes and are bound together as a group identified by a master Node *i* located inside the model; similarly, slave nodes 6 and 7 are also bound together and identified by another master Node *j* located on the model boundary.

2.2 Fracture initiation and propagation

To simulate fracture initiation and propagation, we use the Mohr-Coulomb and maximum tensile strength criteria to simulate both the shear and tensile failures in cFDEM. When a pre-inserted cohesive element is invoked and marked as a yield surface, the master-slave node mapping list and the two groups of slave node linked lists need to be updated accordingly. Continuing with the example shown in Figure 1, and focusing on the master Node *i*, once the cohesive element between Elements E_4 and E_5 becomes a yield surface, the connection between the slave Nodes 3 and 4 will be cut out, and the previous circular linked list becomes an open linked list, such as 4→5→0→1→2→3 (Figure 2a); however, the slave Nodes 0 to 5 are still in the same group and mapped to the same master Node *i* at this time, since they are located at a fracture tip inside the model and have to be enforced to displace together. As the model evolves and another cohesive element is invoked, say, the one between Elements E_6 and E_1, the connection between the slave Nodes 0 and 5 will again be cut out, and the previous open linked list becomes two open linked lists, i.e., 0→1→2→3 and 4→5 (Figure 1b). Then, the slave Nodes 0 to 5 are divided into two groups, and they are respectively mapped to a new master Node *k* and the old master Node *i* (Figure 1b). Further invocation of cohesive elements, e.g., the one between Elements E_2 and E_3 shown in Figure 1c, can be realized by repeating the above procedure. The other nodes of these invoked cohesive elements should also be processed at the same time in a similar manner.

It can be seen that only when a slave node linked list to be cut out is an open list, i.e., the corresponding master node is either located on the model boundaries or connected to an existing yield surface, a new master node is needed to update the master-slave node mapping list and the slave node group lists. Then, the cohesive element starts to participate in the computation, and its mechanical behaviors are controlled by the traction-separation-based strain-softening laws similar to that in ECZM (Lei et al., 2021).

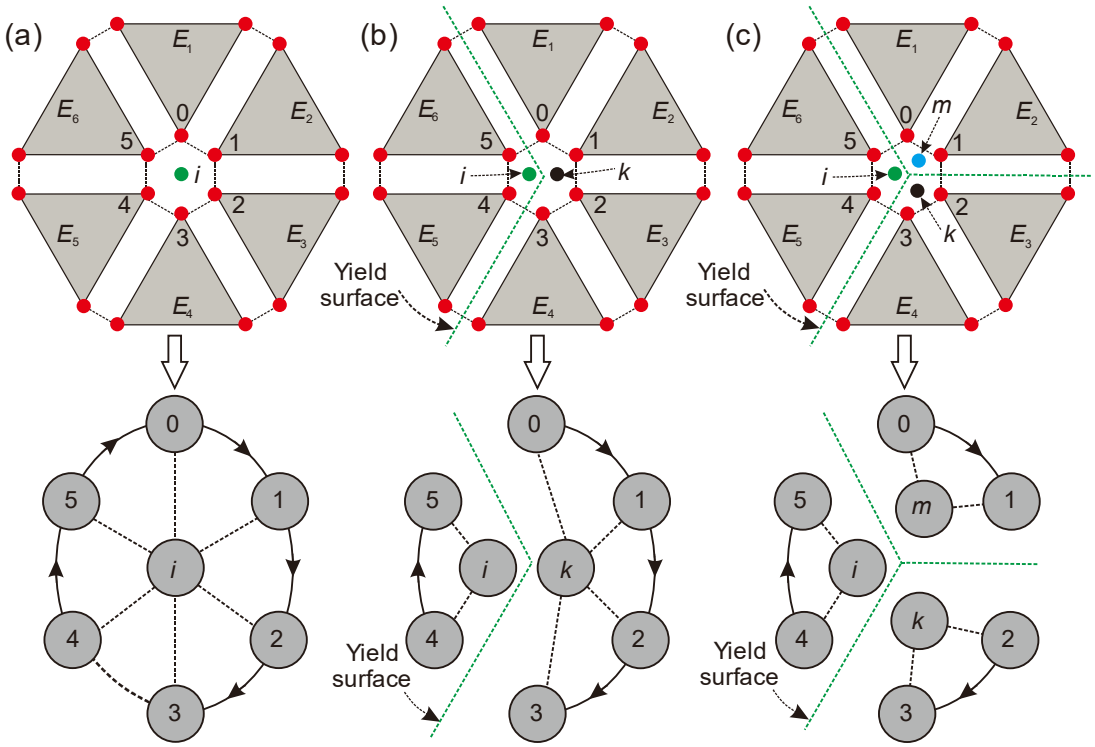

Figure 2. Schematic of updating the master-slave node mapping list and slave node group linked lists when cohesive elements become yield surfaces. The triangular finite elements are marked as E_1, E_2, E_3, E_4, E and E_6 in clockwise order, and Nodes i, k and m are the master nodes used to bind the slave Nodes 0 to 5.

3 VALIDATION AND COMPARISON

In this section, first, a series of tests are performed to test the implementation accuracy of the Mohr-Coulomb and maximum tensile strength criteria. Then, we demonstrate the advantages of the proposed cFDEM compared with the traditional dFDEM in terms of material stiffness.

3.1 Implementation accuracy of strength criteria

To test the implementation accuracy of the Mohr-Coulomb and maximum tensile strength criteria in the proposed cFDEM, a series of triaxial compression and direct tension tests are performed on a rectangular plate presented in Figure 3a-b, where the width and height of the specimen are 50 mm and 100 mm, respectively. The input parameters can refer to previous literature (Deng et al., 2021).

The Mohr-Coulomb criterion in principal stress space is:

$$\sigma_1 = \frac{2c \cdot \cos\varphi}{1-\sin\varphi} + \frac{1+\sin\varphi}{1-\sin\varphi}\sigma_3 \tag{1}$$

where c is the material cohesion, φ is the internal friction angle, and σ_1 and σ_3 are the maximum and minimum principal stresses, respectively. We vary the confining pressure (σ_3) on the two sides of the model from 1 MPa to 6 MPa with a step of 1 MPa (compression positive), and obtain the corresponding peak strength (σ_1). Note that the negative values of σ_3 denote the confining pressure is tensile and the selection of loading rates for the problem fully considers the effect of element size and also ensures an acceptable computation time (Tatone and Grasselli, 2015). The simulated σ_1-σ_3 relations, together with the theoretical curves of the Mohr-Coulomb and maximum tensile strength criteria, are plotted in Figure 3c, which demonstrates a great consistency between the two and thus verifies the capability of cFDEM in simulating tensile and shear failures of rocks.

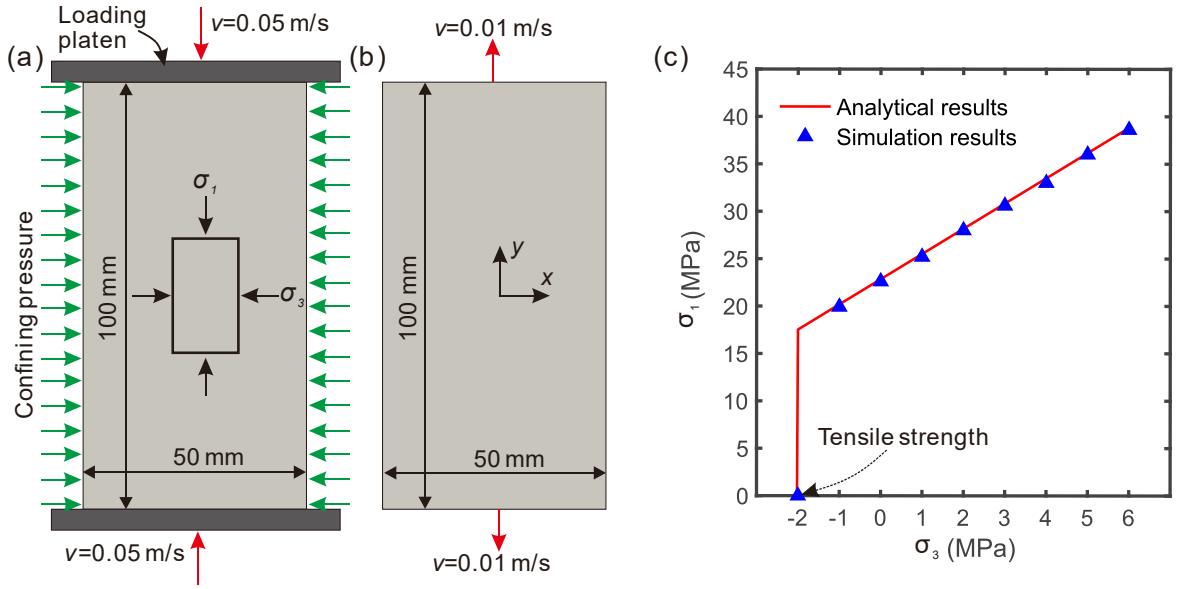

Figure 3. Triaxial compression and direct tension tests. (a) Triaxial compression test. (b) Direct tension test. (c) Comparison between the cFDEM simulated σ_1-σ_3 relations and the theoretical curves of Mohr-Coulomb and maximum tensile strength criteria in principal stress space.

3.2 Material stiffness

As mentioned in previous works (Fan and Tadmor, 2019; Papoulia et al., 2003), the utilization of ICZM in dFDEM can reduce the overall effective modulus of materials (i.e., artificial compliance). Here, a square plate of 30 mm (Figure 4a) is employed to elucidate the material stiffness reduction in dFDEM before fracture onset. We gradually increase the tensile loads acting on both the top and bottom boundaries to $\sigma = 1.0$ MPa and then maintain them unchanged. Here, we use Young's modulus $E = 30$ GPa, Poisson's ratio $\nu = 0.27$, and bulk density $\rho = 2700$ kg/m^3 in the simulations.

To compare the difference between dFDEM and the proposed cFDEM in terms of simulated material stiffness, we vary the ratio (N) between the intrinsic cohesive element penalty parameters and the prescribed Young's modulus of finite elements ($E = 30$ GPa here) from 10 to 100, and calculate the ratio between the simulated macroscopic effective Young's modulus (E_{eff}) and the prescribed Young's modulus of finite elements, i.e., E_{eff}/E. The ratio E_{eff}/E with respect to N is shown in Figure 4b, which effectively demonstrates an overall material stiffness reduction in dFDEM, i.e., $E_{eff}/E < 1$. It can be observed that E_{eff}/E gradually increases with the increment of N, but still less than 1 even for a very large N. Theoretically, the overall material stiffness in dFDEM has no reduction only when the intrinsic cohesive element penalty tends to be infinity; however, in practice, too large a cohesive penalty could lead to spurious traction force oscillations. While for the proposed cFDEM, as shown in Figure 4c, the simulated effective Young's modulus is 30 GPa, which is the same as the prescribed Young's modulus for finite elements, i.e., no material stiffness reduction occurs in our cFDEM model.

4 CONCLUSIONS

In this study, within the framework of cohesive zone model based FDEM, we have proposed a novel continuum-oriented FDEM (cFDEM) using an efficient node binding scheme for rock fracturing simulation. The proposed cFDEM inherits the merits of both ICZM and ECZM, but avoids their shortcomings, and thus provides a novel solution for a more efficient and effective simulation of brittle material evolution from continuum to discontinuum. However, the "time discontinuity" problem in the current FDEM is not well resolved due to the inconsistent constitutive models used for finite elements and cohesive elements in terms of nodal force calculation. Additional work,

referring to the extension of the node binding scheme to 3D rock fracturing simulation, will be reported in the near future.

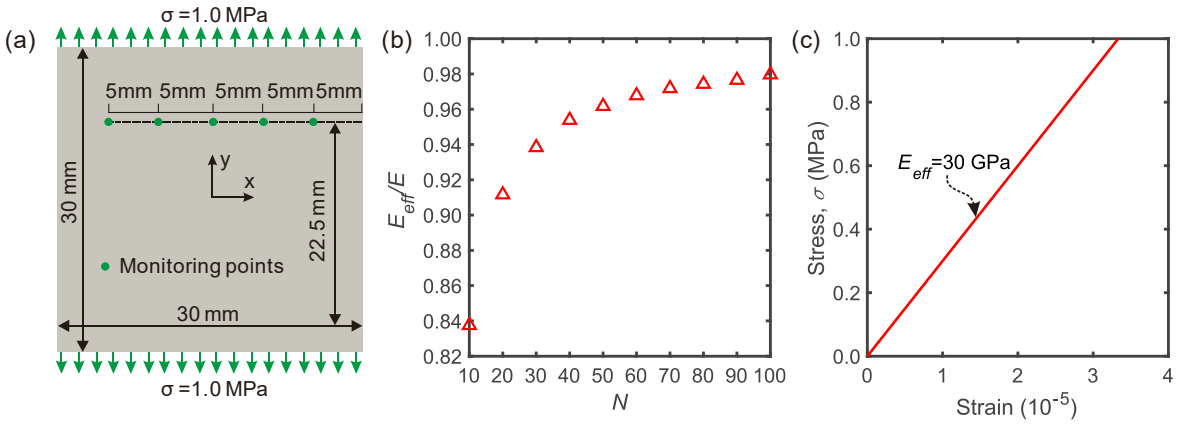

Figure 4. (a) Model setup for simulated material stiffness comparison. (b) The ratio E_{eff}/E varies with N in dFDEM. (c) Stress-strain curve under tensile loading in cFDEM.

ACKNOWLEDGEMENTS

This work is supported by the Shenzhen Science and Technology Program (JCYJ20220530113612028).

REFERENCES

Deng, Penghai, Liu, Quansheng, Huang, Xing, Bo, Yin, Liu, Qi, & Li, Weiwei. 2021. Sensitivity analysis of fracture energies for the combined finite-discrete element method (FDEM). Engineering Fracture Mechanics, 251: 107793

Fan, Jiadi, & Tadmor, E. B. 2019. Rescaling cohesive element properties for mesh independent fracture simulations. Engineering Fracture Mechanics, 213: 89-99

Fukuda, Daisuke, Nihei, Erina, Cho, Sang-Ho, Oh, Sewook, Nara, Yoshitaka, Kodama, Jun-ichi, & Fujii, Yoshiaki. 2020. Development of a Numerical Simulator for 3-D Dynamic Fracture Process Analysis of Rocks Based on Hybrid FEM-DEM Using Extrinsic Cohesive Zone Model. Materials Transactions, 61(9): 1767-1774

Lei, Zhou, Rougier, Esteban, Knight, Earl E., Zang, Mengyan, & Munjiza, Antonio. 2021. Impact Fracture and Fragmentation of Glass via the 3D Combined Finite-Discrete Element Method. Applied Sciences, 11(6): 2484

Munjiza, A. (1992). Discrete elements in transient dynamics of fractured media. Swansea University, Swansea.

Munjiza, A. (2004). The combined finite-discrete element method. London: John Wiley.

Papoulia, Katerina D., Sam, Chin-Hang, & Vavasis, Stephen A. 2003. Time continuity in cohesive finite element modeling. International Journal for Numerical Methods in Engineering, 58(5): 679-701

Tatone, B. S. A., & Grasselli, G. 2015. A calibration procedure for two-dimensional laboratory-scale hybrid finite–discrete element simulations. International Journal of Rock Mechanics and Mining Sciences, 75: 56-72

Xu, Xiao, Wang, Di, Zang, Mengyan, & Chen, Shunhua. 2022. Development of an intrinsic solid-shell cohesive zone model for impact fracture of windshield laminated glass. International Journal of Impact Engineering, 163: 104187